Influences of Metallic Biomaterial Design and Imaging Sequences on Mri Interpretation Challenges Due to Image Artefact

Gulsen AKDOGAN (akdogang@erciyes.edu.tr)
Erciyes University Department of Biomedical Engineering https://orcid.org/0000-0001-6473-8897
Omer Burak ISTANBULLU
Erciyes University: Erciyes Universitesi

Research Article

Keywords: Magnetic Resonance Imaging, Imaging Sequence, Metallic Biomaterials, Magnetic Susceptibility, Image Artefact

Posted Date: July 6th, 2022

DOI: https://doi.org/10.21203/rs.3.rs-1032476/v1

INFLUENCES OF METALLIC BIOMATERIAL DESIGN AND IMAGING SEQUENCES ON MRI INTERPRETATION CHALLENGES DUE TO IMAGE ARTEFACT

Names of the Authors

Gulsen AKDOGAN*, O. Burak ISTANBULLU

Affiliation of the Authors

Department of Biomedical Engineering, Faculty of Engineering, Erciyes University, Kayseri, Turkey

Corresponding Author

*Correspondence to Gulsen AKDOGAN

(akdogang@erciyes.edu.tr)

ORCID of the Authors

Gulsen AKDOGAN

0000-0001-6473-8897

O. Burak ISTANBULLU

0000-0003-3150-9195

Acknowledgments

Funding

This study was supported by funds from the Erciyes University Scientific Research Projects Unit under grant number FYL-2015-6051. The authors would also like to thank ONUR Medical, K. GUMUS and I. KIZILOZ for their support.

Compliance with Ethical Standards

The authors declare that they have no conflict of interest.

This article does not contain any studies with human participants performed by any of the authors.

INFLUENCES OF METALLIC BIOMATERIAL DESIGN AND IMAGING SEQUENCES ON MRI INTERPRETATION CHALLENGES DUE TO IMAGE ARTEFACT

Abstract

Bio-metals cause signal loss and susceptibility artifact at the surrounding tissue resulting in deterioration in the Magnetic Resonance (MR) images. This metal-artifact effect may lead to interpretation challenges for MR images. Therefore, reducing the artifact is required to obtain higher-quality images. This paper aims to analyze the effects of imaging sequence and metallic biomaterial design on MR-image artifacts. With this respect, implant specimens were designed in thin, thick, and pointed forms, manufactured using 316LVM, 316L, CoCr-alloy, and Ti-alloy which are common materials in the biomaterials field. Specimens were placed in a phantom which simulates average human anatomy separately, scanned in a 1.5T MRI under four imaging conditions, "Axial-T1-Gradient-Echo (GRE)", "Sagittal-T1-GRE", "Axial-T2-Spin-Echo (SE)" and "Sagittal-T2-SE". Images were analyzed regarding image artifact amount. It was concluded that the higher magnetic susceptibility of 316LVM SS caused %87 more deterioration than Ti-alloy specimens in the obtained MR images with the mean image artifact to specimen size ratio of 2.77. Thinner designs provided better performance regarding the metal artifact by reducing the artifact to specimen size ratio down to 0.66. T2SE provided obtaining 1.77 times better image quality than T1GRE for clinical interpretation. It can be concluded that image artifact directly depends on material content, geometry, and imaging sequence selection. Minor artifact effect of T2SE provide obtaining more accurate MR images than T1GRE regarding the interpretation of the images of the patients with bio-metal. The higher magnetic susceptibility of bio-metal causes more deterioration of the images.

Keywords: *Magnetic Resonance Imaging; Imaging Sequence; Metallic Biomaterials, Magnetic Susceptibility; Image Artefact*

1. Introduction

Magnetic Resonance Imaging (MRI) technology provides a non-ionizing imaging approach and well-detailed medical images especially for soft tissue imaging with a high resolution. The improved signal-to-noise ratio of MRI technology and obtaining higher quality signal data lead them to be utilized in applications for clinical medicine and practical research [1–3]. MRI technology uses a strong static magnetic field, Radiofrequency (RF) pulses, and gradient magnetic fields to induce MR signals from the body and to generate the images [4, 5]. However, when a metallic material such as a pacemaker, dental or orthopedic implant, vascular stent, or a hip joint existed in the MRI environment, data loss and deterioration occur in the MRI signals during image generation due to the susceptibility differences between the biological tissue and the material [6–8]. Within this regard, Carter et al., Sinclair and Scoffings indicate that despite its unique advantages over other imaging modalities, MRI can be useless for the interpretation of the images nearby the metallic structures such as an implant because of the electromagnetic interaction process at metallic implants and consequences [9, 10]. This interaction depends on both material content, type, geometry, and MRI sequence type. Magnetic susceptibility of the material directly affects the data loss and image artefact amount [11, 12]. Therefore, it is crucial to analyze the electromagnetic influence area of a metallic structure used in the body for orthopedic aspects regarding image artefact to prevent MRI interpretation issues.

1.1. MRI Technology and Imaging Sequences

The abundance of the hydrogen atom allows it to be utilized for obtaining the MR images by the magnetization signals coming from the body [13–15]. The strong static magnetic field and gradient magnetic fields utilized in MRI technology lead hydrogen atoms to align around the magnetic field vector with a resonant frequency [16, 17]. Applying an RF pulse to the region of interest of the body, where aimed to be imaged, causes the magnetic vector to be altered resulting in an electrical signal induction [18]. Sampling and demodulation of the induced electrical signals form a digital matrix which is called k-space. Applying the inverse Fourier transform to the k-space matrix allow obtaining an MR image [19].

An MRI sequence is a group of specified RF pulses that forms the k-space matrix and the image appearance. The imaging sequences which are called Spin Echo and Gradient Echo are commonly used in MRI scans to generate T1-weighted and T2-weighted images [20, 21]. While the T1-weighted image is based on the longitudinal relaxation time differences, the T2-weighted image is based on the transverse relaxation time differences of the magnetic vector between the tissues and structures. All the tissues do not align back around the static magnetic field at the same time after applying the RF pulses, i.e., fat aligns back its longitudinal magnetization in a shorter time than water. This results in contrast differences for different tissues. Therefore, fat appears bright while water is dark in T1 images. This is exactly the opposite in T2 imaging [22]. Two parameters

in an imaging sequence are the repetition time (TR) and the echo time (TE). TR is the time between two RF pulses and TE refers to the time between the RF pulse and the signal peak which is induced in the MRI coil [23, 24]. By varying TR and TE times, different type of MR images can be obtained. While T1 weighting tends to have short TE and TR times, T2 weighting tends to require long TE and TR times [25, 26].

Spin-echo (SE) imaging is one of the most used pulse sequences in MRI. The timing of the pulse sequence can be set to generate both T1 and T2 weighted images. All spin-echo sequences include a 90-degree RF pulse that selects the slice followed by one or multiple 180-degree refocusing RF pulses that prevents signal loss, as shown in Fig. 1(a) [27, 28]. The gradient echo (GRE) is produced by the frequency-encoding gradient pulse in the MR device. GRE sequences consist of 90 degrees or lower RF pulses to generate transverse magnetization as shown in Fig. 1(b). At first, GRE is inverted and used to support dephasing in the transverse direction of the protons, and then afterward, it is used as a readout gradient to align back the de-phased protons and to acquire a strong signal [29]. Due to the low flip angles used in GRE, protection of the longitudinal magnetization occurs as opposed to the 90º pulse used in spin echo, which extinguishes the longitudinal magnetization completely. Consequently, the time of building up for longitudinal magnetization is reduced dramatically for the succeeding pulses to allow image generation in GRE to be faster [30].

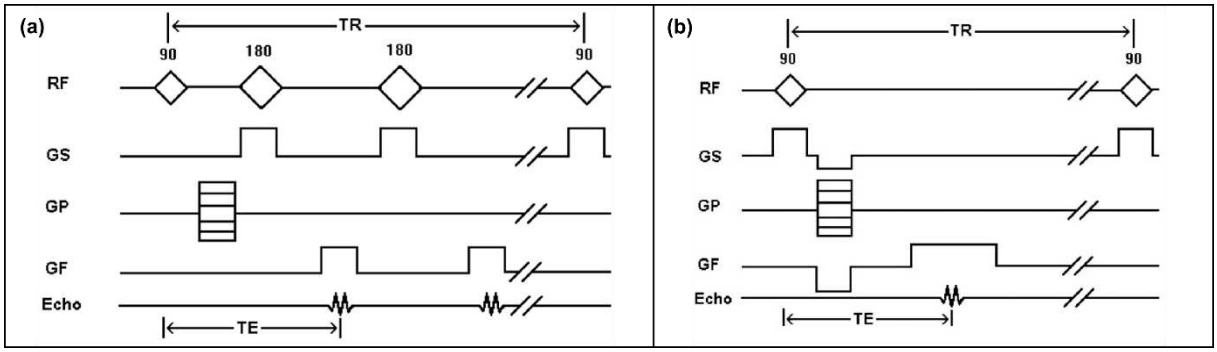

Figure 1. Spin Echo and Gradient Echo sequences used in the experiments

1.2. Metallic Structure Presence in MRI Environment and the Image Artefact Phenomena

Materials that are produced and used for medical purposes are called biomaterials. Biomaterials and implants used in the body are called passive implants or active implants according to their functional properties. While the passive implants provide their functions without any electrical power, the active implants need an electrical circuit system to perform their functions [31]. Biomaterials are designed as having different mechanical, chemical, or optical features because of the varying usage region in the human body such as the eye, veins, dental region, femur, or patella. All the biomaterials to be used in the human body must be biocompatible but different physical properties are expected from varying biomaterial types [32, 33]. Metallic biomaterials called bio-metals are used thanks to their mechanical, biological, or electrical properties. A bio-metallic implant can be manufactured using different types of alloys depending on the region where the implant will be placed in.

316L and 316LVM low carbon alloy Stainless Steel (316L SS and 316LVM SS), CoCr alloys, and Ti alloy materials are commonly used in the production of artificial hip prostheses, bone plates/screw, heart valves, stents, and dental implants due to their advantages such as ductility, impact strength and wear resistance [34, 35]. The alloy elements used in metallic implants affect the magnetic properties of the implant due to the magnetic susceptibilities of the contained elements, leading to the implant being MRI-compatible, MRI-conditional, or MRI-hazardous [36]. The implants having diamagnetic features are generally considered compatible with the MRI system because the magnetic force induction due to the external magnetic field exposure for diamagnetic materials is very low. Therefore, while the diamagnetic material is under the influence of the magnetic field, deflection is not expected for an implant which is placed in a body region [37]. However, metallic implants may also contain ferromagnetic elements such as Fe, Ni, and Co. Depending on the amount of these elements in the implant production, the implant may be ferromagnetic. Therefore, such materials with a ferromagnetic feature are not allowed to be in the MRI environment due to the MRI safety issues arise from magnetic deflection, torque or overheating [38].

In addition to the MRI safety of a metallic implant, image artefact in the tissue nearby the bio-metal may also occur for the patients with a metallic implant depending on the alloy element content and implant's magnetic feature [39, 40]. The atoms of the tissue or metallic structure placed in a magnetic field form a magnetic moment vector due to their spin motion. The value of an atom's Magnetic Moment (μ) depends on the Larmor Constant (γ) and Spin Angular Momentum (J) of each atom. The Larmor constant is also called Gyromagnetic Ratio. This ratio is determined with Eq. (1), by the ratio of the Magnetic Dipole Moment to the Angular Momentum, and the Larmor constant is specific for each element [41].

$$\gamma = \frac{\mu}{J} \quad (1)$$

The rotation quantity of an atom in a magnetic field at a certain time is called precession frequency or the Larmor frequency which is expressed by *w*. The value of the frequency varies with the magnitude of the applied magnetic field and the Larmor constant [41]. The mathematical expression of Larmor frequency is given with Eq. (2).

$$w = \gamma . B_0 \quad (2)$$

There is a direct relationship between the MR image and k-space matrix data which is formed by the induced signals coming from the body region of interest. The magnetic susceptibility of a metallic structure is generally dominant to the biological tissue; therefore, it may result in signal suppression leading to the region nearby the metal becoming deteriorated and blurred in the MR images [42, 43]. Therefore, bio-metals' compatibility with the imaging device is crucial to prevent image interpretation issues due to image deterioration.

Due to the metallic biomaterials used in the body are produced using various alloys, orthopedic implant specimens made of 316LVM SS, 316L SS, CoCr Alloy, and Ti-alloy (Ti6Al4V) were obtained from the manufacturers for analyzing the effects of the material content and geometry on MR image artefact in this study. With this regard, the specimens were designed and manufactured in thin, thick, and pointed forms. The specimens' content was determined considering their common usage in orthopedics and dental applications. All the specimens were placed in a phantom that mimics the magnetic, electrical, and thermal features of an average human body. The implant-placed phantom was scanned in a 1.5T MRI device using 4 different MRI sequences which are "Axial T1 Gradient-Echo", "Sagittal T1 Gradient-Echo", "Axial T2 Spin-Echo" and "Sagittal T2 Spin-Echo". Related ASTM standards are used for analyzing and comparing the metal-artefact effects.

2. Materials and Methods

2.1. Designing and Manufacturing the Implant Specimens

Considering the orthopedic and dental implants are produced in varying sizes and shapes for clinical aspects, three different implant specimens which are thin, thick, and plotted shapes were designed in CATIA® software as seen in Fig. 2. The designs were determined to provide an effective geometric comparison for MRI-image artefact analysis.

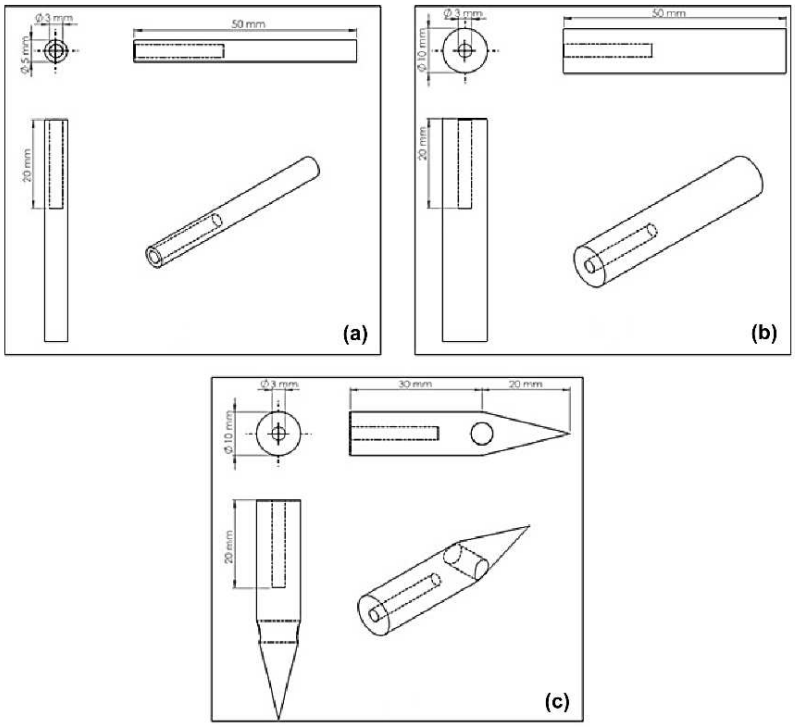

Figure 2. Implant specimen modelling in CATIA software

Modelled specimens were manufactured using 316L SS, 316LVM SS, CoCr alloy and Ti-alloy (Ti-6Al-4V) which are commonly used bio-metals in orthopedics and dental applications to analyze the influences of material contents on obtained MR images. A total number of 12 specimens having 3 geometries using 4 alloy materials were obtained for performing the experiments. Chemical analysis of the manufactured specimens was applied with XRF Analyzer (X-Ray Fluorescence) as shown in Table-1.

Table 1. Chemical composition and XRF analysis results of four orthopedic implant test specimens

Specimen Name	Content		Specimen Name	Content	
	Element	Ratio		Element	Ratio
Titanium Alloy	*Ti*	*96.77*	*316LVM Stainless Steel*	*Fe*	*63.838*
	Fe	*2.74*		*Cr*	*18.620*
	Cu	*0.38*		*Ni*	*13.201*
	Si	*0.06*		*Mo*	*2.689*
	Al	*0.06*		*Mn*	*1.652*
316L Stainless Steel	*Fe*	*67.916*	*CoCr Alloy*	*Co*	*63.0*
	Cr	*17.062*		*Cr*	*27.86*
	Ni	*10.358*		*Mo*	*6.20*
	Mo	*2.019*		*Mn*	*0.52*
	Mn	*1.478*		*Si*	*0.63*
	Cu	*0.505*		*Fe*	*0.37*
	Si	*0.325*		*C*	*0.37*
	Co	*0.143*		*Ni*	*0.32*
	C	*0.065*		*N*	*0.29*
	Nb	*0.031*		*W*	*0.20*
	V	*0.028*		*Al*	*0.10*
	S	*0.025*		*Ti*	*0.10*
	P	*0.023*		*P*	*0.02*
	Al	*0.012*		*B*	*0.01*
	Ti	*0.010*		S	0.01
The XRF analyses were performed at Erciyes University Technology Research and Application Centre					

2.2. Analysis Conditions and Imaging Sequences

All twelve specimens were placed separately in a phantom that simulates the average human body's thermal and electrical properties. Phantom-implant system was scanned in 1.5T MRI device (Magnetom, Siemens) using four imaging sequences which are "Axial T1 Gradient-Echo", "Sagittal T1 Gradient-Echo", "Axial T2 Spin-Echo" and "Sagittal T2 Spin-Echo". All the obtained images were analyzed in terms of image artefact quantity. ASTM F-2119 standard was used as a reference in evaluating how material content, shape, and size of an implanted material affects MR image artefact. First, test specimens that are safe to use in the MR environment were distinguished [44]. For this purpose, the magnetic force measurement analysis which is specified in ASTM F 2052 standard has been applied to all test specimens [45]. 316L SS and CoCr alloy specimens were found to be unsafe due to the presence of magnetic force and deflection occurrence when placed in an MRI environment. There was no magnetic force formation for the specimens made of 316LVM and Ti-alloy, therefore these specimens were placed in the phantom and scanned using 4 different MRI sequences during the 10-minute period, respectively. Phantom without any metallic implant was also scanned in the same conditions for comparison of the image artefact amount. Gradient Echo (T1GRE) and T2 Spin Echo (T2SE) sequences are used in most of the MRI scan in clinical applications. For this reason, these imaging sequences with ten-minutes duration in the axial and sagittal plane were chosen during the analyses. The Time of Repetition (TR) and Time of Echo (TE) values of the sequences used during analysis are shown in Table 2.

Table 2. Time of Repetition (TR), Time of Echo (TE), and Specific Absorption Rate (SAR) values of MRI sequences

Sequence	Slice	TR (ms)	TE (ms)	SAR (W/kg)
T1GRE	Axial	2070	2.9	0.15
	Sagittal	2200	2.9	0.16
T2SE	Axial	4400	95	0.17
	Sagittal	4380	95	0.17

3. Results

T1GRE sagittal (a), T2SE sagittal (b), T1GRE axial (c), and T2SE axial (d) images were obtained from the phantom which included thin-designed implants, thick-designed implants, and pointed-designed implant specimens which were manufactured using 316LVM SS and Ti alloy are given in Fig. 3, Fig. 4, and Fig. 5, respectively. The obtained MR images of the phantom including 316LVM SS and Ti alloy implant specimens were compared with the images of the empty phantom without a metallic implant regarding image artefact amount.

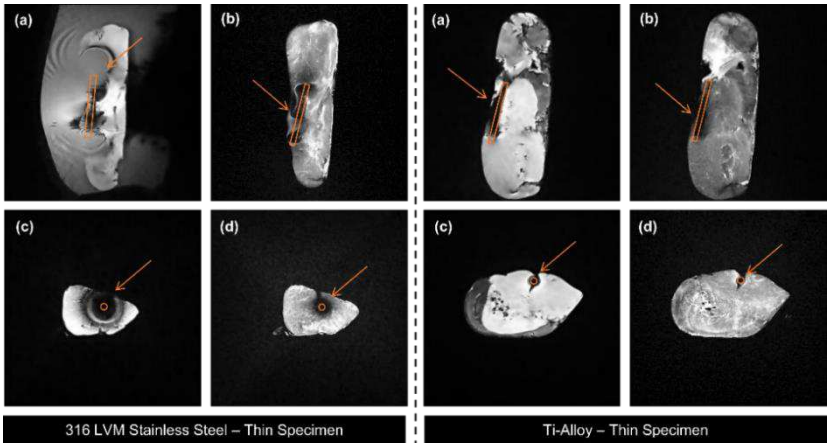

Figure 3. MR images of thin-designed 316LVM SS and Ti-alloy placed phantom: T1GRE sagittal (a), T2SE sagittal (b), T1GRE axial (c) and T2SE axial (d).

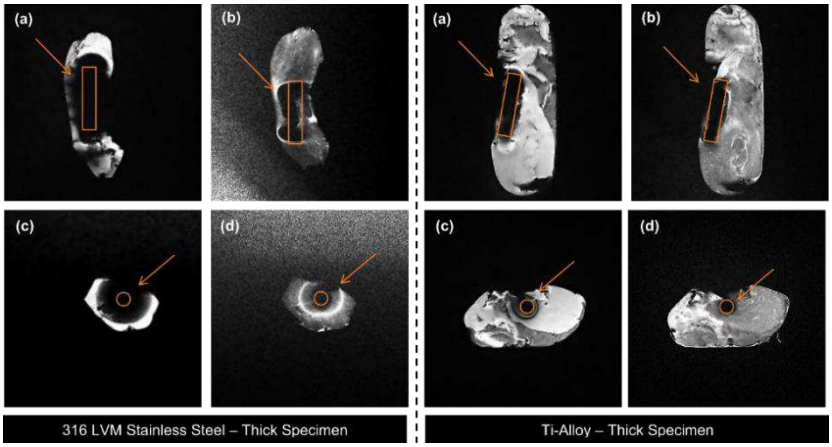

Figure 4. MR images of thick-designed 316LVM SS and Ti-alloy placed phantom: T1GRE sagittal (a), T2SE sagittal (b), T1GRE axial (c) and T2SE axial (d).

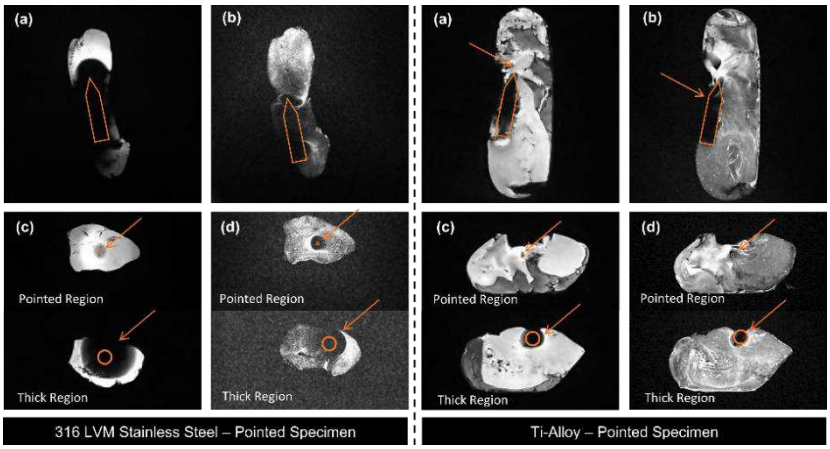

Figure 5. MR images of pointed-designed 316LVM SS and Ti-alloy placed phantom: T1GRE sagittal (a), T2SE sagittal (b), T1GRE axial (c) and T2SE axial (d).

When the images are examined, it was observed that all the specimens with metal contents caused signal loss around the specimens, which led to deterioration in the image depending on both the material content and geometry of the specimens. Image artefact quantities were calculated in MATLAB by the ratio of deterioration amount nearby the specimen and implant's size. The calculated image artefact amounts are given in Table 3. The proportional values in the table are the ratio of the region where the signal loss in the MRI image occurred and the surface area of the implanted specimen. A comparison of image artefact to implant size depending on material type, model, and imaging sequences is given in Fig. 6.

Table 3. Image artefact quantities of MR-safe implant specimens in four different imaging sequences

Implant Specimen			**Image artefact to implant size ratio***			
			Sagittal Plane		**Axial Plane**	
Specimen Name	**Specimen Geometry**		**T1GRE**	**T2SE**	**T1GRE**	**T2SE**
316LVM Stainless Steel	Thin		3.055	2.047	12.337	8.669
	Thick		2.409	0.988	17.347	6.563
	Pointed	Sharp Region	3.456	3.255	20.886	18.750
		Coarse Region	2.160	0.465	12.820	2.637
Titanium Alloy	Thin		0.403	0.137	1.202	0.881
	Thick		0.490	0.082	4.670	0.707
	Pointed	Sharp Region	0.334	0.682	3.795	3.125
		Coarse Region	0.197	0.149	2.233	0.389
* The proportional value is the ratio of the region where the signal loss occurred to the size of the implanted specimen.						

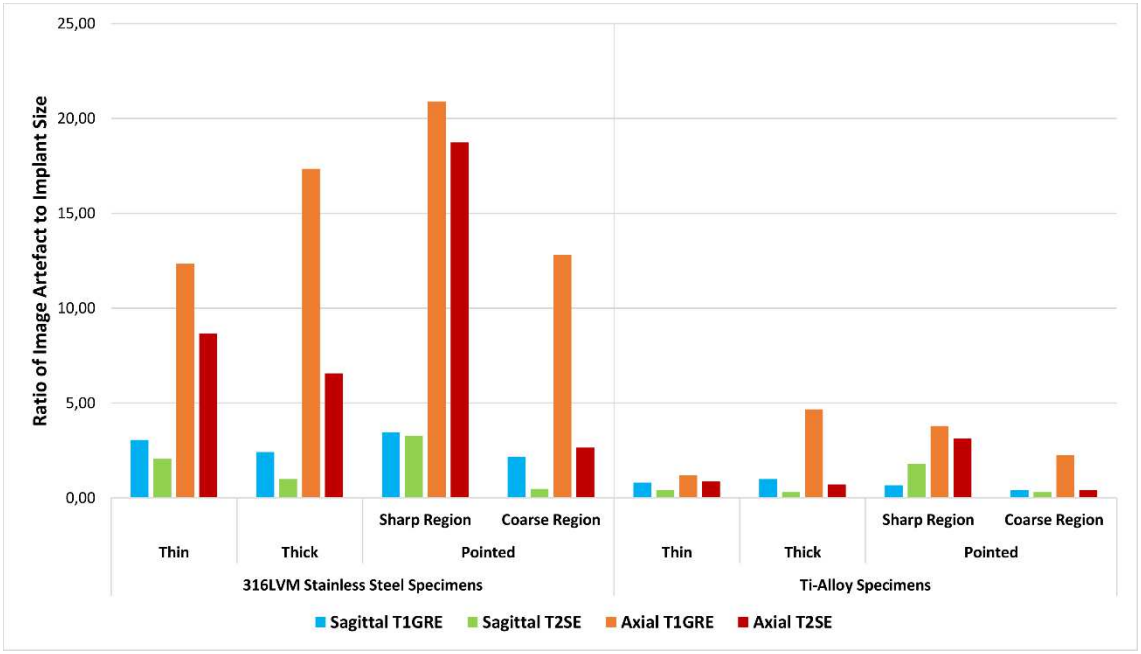

Figure 6. Ratio of image artefact to implant size depending on material type, shape, and imaging sequences

The increasing image artefact amount due to the influence of susceptibility effect area for the specimens having different geometries and contents can be clearly seen from the obtained figures and calculations. It was observed that 316LVM SS, which includes a very high ratio of ferromagnetic Fe element, caused more deterioration than the Ti-alloys in the MR images. When the axial and sagittal planes of the T1GRE and T2SE sequences of the same specimens were analyzed, a lower image distortion occurrence nearby the placed implant for T2SE sequence was obtained when compared to T1GRE sequence. It is considered by the usage of 180º dephasing RF pulse in T2SE prevented the signal loss nearby the metallic structure.

4. Discussion

In this study, implants were designed in three different forms and manufactured using four different bio-metals which are commonly used in orthopedics and dental applications. All specimens were analyzed in terms of MRI safety using ASTM F-2052 standard and 316L SS and CoCr alloy specimens were found as MRI-unsafe due to the magnetic deflection formation. Implant specimens made of 316LVM SS and Ti-alloy were placed in a phantom that simulates an average human body's thermal and electrical properties. The Implant-phantom system was scanned in a 1.5 T MRI device using 4 different imaging sequences which are commonly used in clinical applications. Obtained MRI images are analyzed in MATLAB using image processing techniques in terms of image artefact quantity as seen in Table 3.

Mean image artefact ratios were calculated using the observed values. It was observed that the artefact ratio for was less for Ti-alloy specimens with an amount of 0.36, than the 316LVM SS specimens with a value of 2.77 in the obtained MR images using the T1GRE sequence in the sagittal plane. The image artefact size for the T2SE sequence in the sagittal plane was observed as 0.26 for Ti-alloy, and 1.69 for 316LVM SS. While the maximum image artefact ratio occurred for 316LVM SS for the images obtained using T1GRE sequence in the axial plane with a value of 20.886, the minimum image artefact ratio was observed for the Ti-alloy specimens in the MR images obtained using the T2SE sequence in the sagittal plane with a value of 0.149. The findings indicate that the image artefact size depends on both material content and selected sequence type. This is because of the magnetic susceptibilities of the elements used in 316LVM production which is stronger than the Ti-alloy implant due to the dominance of ferromagnetic contents. Therefore, the precession of 316LVM SS atoms caused more signal loss and deterioration in the images than Ti-alloy specimens.

When the specimen geometries were compared, it can be concluded that the mean image artefact ratios were calculated as 0.66 for thin-designed, 1.49 for thick-designed, and 1.36 for pointed-designed Ti-alloy specimens. The same calculation was performed for 316LVM SS and the image artefact ratio was 6.53 for thin-designed, 6.83 for thick-designed, and 8.05 for pointed-designed specimens. As seen from the findings, specimen and implant geometry is another parameter in the image artefact effect for MR imaging for the patients with metallic biomaterials. The thinner geometries resulted in less deterioration in obtained MR images.

Another result that can be concluded from Table 3 is that the imaging sequence also influences image artifacts. Mean values of image artefact ratio depending on the selected imaging sequence were calculated. The mean ratio was observed as 5.48 for the T1GRE sequence and 3.1 for the T2SE sequence. As seen from the calculations, it can be clearly seen that the deteriorations in the images of the axial and sagittal T1GRE sequences obtained from the same specimens were higher than the T2SE sequence. This is due to the 180º dephasing RF pulse was utilized in the T2SE sequence which reduced the signal loss, distortion, and image artifact. Therefore, it was achieved that the scanning of patients with metallic implants by using the T2SE sequence will make the image interpretation to be more accurate than the T1GRE sequence.

5. Conclusion

It can be concluded that increasing implant size leads to higher total magnetic susceptibility which causes more signal loss and image artefact nearby the metallic structure leading to deterioration in the MR images. The ferromagnetic content of the metallic structure results in more artefacts than diamagnetic structures for MR images. Obtaining the MR images using the T2SE sequence decreases image artifacts of the same material type and model, thanks to the utilization of dephasing RF pulses.

This study demonstrates that metallic implants which are commonly used in orthopedics affect the images generated by MRI scan. The amount of image artefact depends on both material content and imaging sequence. It can be concluded from this study that, because of the lower image artifact which occurs in the T2SE sequence from soft tissue around the implant, MRI scanning of metallic implant carrying patients with this sequence will make the image interpretation more accurate than T1GRE imaging because of minor artifact effect which occurs in this sequence. Besides, the higher magnetic susceptibility of 316LVM causes more deterioration than Ti-alloy which may lead to the difficult interpretation of MRI.

Statements and Declarations

Funding

This study was supported by funds from the Erciyes University Scientific Research Projects Unit under grant number FYL-2015-6051. The authors would also like to thank ONUR Medical, K. GUMUS and I. KIZILOZ for their support.

Compliance with Ethical Standards

The authors declare that they have no conflict of interest.

This article does not contain any studies with human participants performed by any of the authors.

References

1. Brown RW, Cheng Y-CN, Haacke EM, et al (2014) Magnetic Resonance Imaging: Physical Principles and Sequence Design
2. Liang Z-P, Lauterbur PC (2000) Principles of magnetic resonance imaging: a signal processing perspective [Book Review]. Wiley-IEEE Press
3. Lakshmeeha T, Ajith Kumar KS, Vishanth SC, Kiran SC (2019) Study of correlation between clinical findings, radiological and intra operative findings in lumbar disc prolapse. Int J Orthop Sci 5:65–68. https://doi.org/10.22271/ortho.2019.v5.i3b.1509
4. Nacher PJ, Kumaragamage S, Tastevin G, Bidinosti CP (2020) A fast MOSFET rf switch for low-field NMR and MRI. J Magn Reson 310:. https://doi.org/10.1016/j.jmr.2019.106638
5. Vinding MS, Skyum B, Sangill R, Lund TE (2019) Ultrafast (milliseconds), multidimensional RF pulse design with deep learning. Magn Reson Med 82:. https://doi.org/10.1002/mrm.27740
6. Galley J, Sutter R, Stern C, et al (2020) Diagnosis of periprosthetic hip joint infection using MRI with metal artifact reduction at 1.5 T. Radiology 296:. https://doi.org/10.1148/radiol.2020191901
7. Wimmer W, Hakim A, Kiefer C, et al (2019) MRI Metal artifact reduction sequence for auditory implants: First results with a transcutaneous bone conduction implant. Audiol Neurotol 24:. https://doi.org/10.1159/000500513
8. Hargreaves BA, Worters PW, Pauly KB, et al (2011) Metal-induced artifacts in MRI. Am J Roentgenol 197:. https://doi.org/10.2214/AJR.11.7364
9. Sinclair AG, Scoffings DJ (2010) Imaging of the post-operative cranium. Radiographics 30:. https://doi.org/10.1148/rg.302095115
10. Carter LN, Addison O, Naji N, et al (2020) Reducing MRI susceptibility artefacts in implants using additively manufactured porous Ti-6Al-4V structures. Acta Biomater 107:. https://doi.org/10.1016/j.actbio.2020.02.038
11. Smith MR, Artz NS, Wiens C, et al (2015) Characterizing the limits of MRI near metallic prostheses. Magn Reson Med 74:1564–1573. https://doi.org/10.1002/mrm.25540
12. Daga P, Pendse T, Modat M, et al (2014) Susceptibility artefact correction using dynamic graph cuts: Application to neurosurgery. Med Image Anal 18:1132–1142. https://doi.org/10.1016/j.media.2014.06.008
13. Akçakaya M, Tang M, Nezafat R (2019) Cardiac Magnetic Resonance Imaging. In: Kwong RY, Jerosch-Herold M, Heydari B (eds) Cardiovascular Magnetic Resonance Imaging, 2nd ed. Springer, New York, NY, pp 1–16
14. Sands MJ, Levitin A (2004) Basics of magnetic resonance imaging. Semin Vasc Surg 17:66–82
15. Fong W (2005) Handbook of MRI Pulse Sequences. Med Phys 32:1452–1452. https://doi.org/10.1118/1.1904597
16. Deichmann R, Nöth U, Weiskopf N (2010) The basics of functional magnetic resonance imaging. In: EEG - fMRI: Physiological Basis, Technique, and Applications
17. Stafford R (2017) The spin-echo sequence; K-space. Med Phys 44:
18. Schenck JF (2005) Physical interactions of static magnetic fields with living tissues. Prog Biophys Mol Biol 87:185–204. https://doi.org/10.1016/j.pbiomolbio.2004.08.009
19. Wolbarst A (2015) TU-EF-BRA-01: NMR and Proton Density MRI of the 1D Patient. Med Phys 42:. https://doi.org/10.1118/1.4925678
20. Khajehim M, Christen T, Tam F, Graham SJ (2021) Streamlined magnetic resonance fingerprinting: Fast whole-brain coverage with deep-learning based parameter estimation. Neuroimage 238:. https://doi.org/10.1016/j.neuroimage.2021.118237
21. Khajehim M, Christen T, Chen JJ (2019) Magnetic Resonance Fingerprinting with Combined Gradient- And Spin-echo Echo-planar Imaging: Simultaneous Estimation of T1, T2 and T2* with integrated-B1 Correction. bioRxiv. https://doi.org/10.1101/604546
22. Jaubert O, Cruz G, Bustin A, et al (2021) T1, T2, and Fat Fraction Cardiac MR Fingerprinting: Preliminary Clinical Evaluation. J Magn Reson Imaging 53:. https://doi.org/10.1002/jmri.27415
23. Sharma, H. A., & Lagopoulos J (2010) MRI physics : pulse sequences. Acta Neuropsychiatr 22:90–92
24. Eckstein F, Burstein D, Link TM (2006) Quantitative MRI of cartilage and bone: Degenerative changes in osteoarthritis. NMR Biomed. 19
25. Deka B, Datta S (2019) Introduction to Compressed Sensing Magnetic Resonance Imaging
26. Weishaupt D, Kochli VD, Marincek B, Kim EE (2007) How Does MRI Work? An Introduction to the Physics and Function of Magnetic Resonance Imaging. J Nucl Med 48:. https://doi.org/10.2967/jnumed.107.045104
27. Chen F, Taviani V, Malkiel I, et al (2018) Variable-density single-shot fast spin-echo MRI with deep learning reconstruction by using variational networks. Radiology 289:. https://doi.org/10.1148/radiol.2018180445
28. Loening AM, Saranathan M, Ruangwattanapaisarn N, et al (2015) Increased speed and image quality in single-shot fast spin echo imaging via variable refocusing flip angles. J Magn Reson Imaging 42:. https://doi.org/10.1002/jmri.24941
29. Kadamangudi S, Reutens D, Sood S, Vegh V (2018) Signal compartments in ultra-high field multi-echo gradient echo MRI reflect underlying tissue microstructure in the brain. Neuroimage 178:. https://doi.org/10.1016/j.neuroimage.2018.05.061
30. Markl M, Leupold J (2012) Gradient echo imaging. J Magn Reson Imaging 35:1274–1289. https://doi.org/10.1002/jmri.23638
31. Virtanen H, Keshvari J, Lappalainen R (2006) Interaction of radio frequency electromagnetic fields and passive metallic implants - A brief review. Bioelectromagnetics 27:431–439
32. Istanbullu OB, Akdoğan G (2016) Evaluation of MRI compatibility and safety risks for biomaterials. In: 2015 Medical Technologies National Conference, TIPTEKNO 2015
33. Ratner BD, Hoffman AS, Schoen FJ, Lemons JE (2013) Biomaterials Science: An Evolving, Multidisciplinary Endeavor, Third Edit. Elsevier
34. Agten CA, Del Grande F, Fucentese SF, et al (2015) Unicompartmental knee arthroplasty MRI: impact of slice-encoding for metal artefact correction MRI on image quality, findings and therapy decision. Eur Radiol 25:2184–2193. https://doi.org/10.1007/s00330-015-3596-4

35. Park J, Lakes RS (2007) Biomaterials: An introduction: Third edition
36. Poh PG, Liew C, Yeo C, et al (2017) Cardiovascular implantable electronic devices: a review of the dangers and difficulties in MR scanning and attempts to improve safety. Insights Imaging 8
37. Xuan X (2019) Recent advances in continuous-flow particle manipulations using magnetic fluids. Micromachines 10
38. Schenck JF (2000) Safety of strong, static magnetic fields. J Magn Reson Imaging 12:2–19. https://doi.org/10.1002/1522-2586(200007)12:1<2::AID-JMRI2>3.0.CO;2-V
39. Ozawa E, Honda E ichi, Parakonthun KN, et al (2018) Influence of orthodontic appliance-derived artifacts on 3-T MRI movies. Prog Orthod 19:. https://doi.org/10.1186/s40510-018-0204-6
40. Krupa K, Bekiesińska-Figatowska M (2015) Artifacts in magnetic resonance imaging. Polish J Radiol 80:. https://doi.org/10.12659/PJR.892628
41. Choi JS, Kim S, Yoo D, et al (2017) Distance-dependent magnetic resonance tuning as a versatile MRI sensing platform for biological targets. Nat Mater 16:. https://doi.org/10.1038/nmat4846
42. Lee YH, Hahn S, Kim E, Suh J-S (2016) Fat-suppressed MR Imaging of the Spine for Metal Artifact Reduction at 3T: Comparison of STIR and Slice Encoding for Metal Artifact Correction Fat-suppressed T2-weighted Images. Magn Reson Med Sci XX:1–8. https://doi.org/10.2463/mrms.mp.2015-0055
43. Greenbaum B, Barnes FS (2018) Bioengineering and Biophysical Aspects of Electromagnetic Fields. CRC Press
44. ASTM (American Society of Testing and Materials) (2015) ASTM F2119: Standard Test Method for Evaluation of MR Image Artifacts from Passive Implants. West Conshohocken
45. ASTM (American Society of Testing and Materials) (2015) Standard test method for measurement of radio frequency induced heating near passive implants during magnetic resonance imaging. West Conshohocken